Hindawi Publishing Corporation
Journal of Nanotechnology
Volume 2014, Article ID 349453, 11 pages
http://dx.doi.org/10.1155/2014/349453

Research Article

Peeling of Long, Straight Carbon Nanotubes from Surfaces

Kane M. Barker,[1] Mark A. Poggi,[1] Leonardo Lizarraga,[1] Peter T. Lillehei,[2] Aldo A. Ferri,[3] and Lawrence A. Bottomley[1]

[1] *School of Chemistry and Biochemistry, Georgia Institute of Technology, Atlanta, GA 30332-0400, USA*
[2] *Advanced Materials and Processing Branch, NASA Langley Research Center, Hampton, VA 23681-2199, USA*
[3] *George W. Woodruff School of Mechanical Engineering, Georgia Institute of Technology, Atlanta, GA 30332-0405, USA*

Correspondence should be addressed to Lawrence A. Bottomley; bottomley@gatech.edu

Received 15 July 2013; Accepted 20 December 2013; Published 23 February 2014

Academic Editor: Bobby G. Sumpter

Copyright © 2014 Kane M. Barker et al. This is an open access article distributed under the Creative Commons Attribution License, which permits unrestricted use, distribution, and reproduction in any medium, provided the original work is properly cited.

The adhesion of long, straight, single-walled carbon nanotubes to surfaces is examined using multidimensional force spectroscopy. We observed characteristic signatures in the deflection and frequency response of the cantilever indicative of nanotube buckling and slip-stick motion as a result of compression and subsequent adhesion and peeling of the nanotube from the surface. The spring constant and the elastic modulus of the SWNT were estimated from the frequency shifts under tension. Using elastica modeling for postbuckled columns, we have determined the static coefficient of friction for the SWNT on alkanethiol-modified gold surfaces and showed that it varies with the identity of the monolayer terminal group.

1. Introduction

The atomic force microscope (AFM) is an important tool in the characterization of the structure and mechanical properties of carbon nanotubes (CNTs) [1–3]. The tensile strength and bending properties of both single- and multi-walled carbon nanotubes have been determined with this instrument. The high aspect ratio and small effective radius of CNTs provided impetus for attaching or growing them onto the apex of cantilever tips. Indeed, carbon nanotube tips are now important probes in atomic force microscopy [4–6]. They offer significantly improved image resolution and enable imaging of surfaces with deep crevices and trench structures [7–9].

The elastic buckling property of nanotubes is both an advantage and a limitation when used as a scanned probe [2, 10]. Imaging with an unbuckled CNT-tip provides enhanced feature resolution compared to conventional silicon or silicon nitride tips. Imaging with a buckled CNT-tip reduces the force applied while imaging soft samples but with loss in image resolution. Several recent reports have documented the challenges associated with these tips [2, 8, 10–16].

Under certain conditions, buckled CNT-tips will either slide freely across the surface or slip and then stick at specific locations on the surface [17–20]. Indeed, surface roughness and composition play a large role in determining which phenomenon will take place. When imaging with nanotube tipped probes, it is common practice to monitor up to three different outputs from the AFM: cantilever deflection, oscillation amplitude [12, 21–26], and/or phase versus the extent of scanner motion [5, 12, 23, 27–30]. Acquisition of oscillation amplitude and phase data requires that a mechanical perturbation be imposed on the system. Tracking either oscillation amplitude or phase is, in fact, monitoring the system response at a single frequency and can often provide misleading information and engender incomplete interpretation of the mechanical response of the nanotube. Thus, a more systematic method for determining when buckling and slip or slip-stick motion event takes place is needed.

We report herein an improved method for determining when buckling and slip-stick events occur. This method involves the simultaneous monitoring of cantilever deflection and thermal resonance during cycled movement of the AFM

scanner [17, 18, 30]. Changes in resonance frequency and amplitude for several flexural modes of cantilever vibration provide information about the nanotube's response to compressive load (i.e., buckling and slip-stick motion), tip-surface interactions that may be present, and a more straightforward means for quantifying the CNT's mechanical properties [31–35]. Since comparison of the frequency response with force curve data adds an additional dimension of information to traditional force curve analysis, we will hereafter refer to this method as *multidimensional force spectroscopy*, MDFS.

We also present herein an examination of the response of long CNT-tips to compressive loading on several chemically modified substrates: (i) 1-undecanethiol, (ii) 11-hydroxy-undecanethiol, and (iii) 11-amino-undecanethiol. Buchoux et al. [17, 18] have previously examined axial compression of SWNT on graphite and mica substrates. We present herein new evidence that adhesion between the surface and the nanotube-modified AFM tip can significantly alter the mechanical behavior of the nanotube [36]. Finally, we identify characteristic signatures in the deflection and frequency response of the cantilever that indicate buckling and slip-stick events of the CNT under compression and its adhesion to the surface under tension.

2. Experimental

Cantilevers with long, single-walled nanotubes attached to the probe tip were purchased from NanoDevices. These SWNT modified tips were fabricated using a chemical vapor deposition method similar to that previously described [37]. Attachment of the SWNT to the tip is assured by patterned deposition of the catalyst onto the tip and direct growth of the nanotube onto the catalyst. Prior to and following the AFM studies described herein, each tip was examined with a LEO 1550 scanning electron microscope (Carl Zeiss SMT Inc., Thornwood, NY, USA). Accelerating voltages were kept below 10 kV to reduce nanotube vibration and minimize damage from exposure to the electron beam.

Two types of substrates were used herein: silicon ⟨100⟩ chips and chemically modified template-stripped gold. The silicon chips were cleaned with hot aqueous Piranha solution (7 : 3 $H_2SO_4 : H_2O_2$), rinsed in filtered absolute ethanol, and then stored in a desiccator until use. Freshly prepared template-stripped gold substrates were immersed into 2 mM solutions of one of the following alkanethiols dissolved in filtered absolute ethanol: 1-undecanethiol, 11-hydroxy-undecanethiol, and 11-amino-undecanethiol (the first two were used as received from Sigma-Aldrich; the last was used as received from Dojindo Chemicals). After 2 hours, the modified gold substrates were removed from solution, rinsed in filtered absolute ethanol, and then stored in a desiccator until use.

A Veeco Instruments NanoScope IIIa scanning probe microscope with extender electronics and signal access module was used for all force spectroscopic measurements. The piezo scanner was calibrated in x, y, and z using NIST certified calibration gratings (MikroMasch, San Jose, CA, USA). To initiate each experiment, the cantilever-SWNT probe was mounted in the holder and placed in the AFM. Image acquisition was commenced without allowing contact between the probe and the substrate surface. The microscope was then placed in force spectroscopy mode and the scanner was cycled in the z-direction for 2 hr under constant flow of nitrogen (2 L min^{-1}) to allow the system to reach thermal equilibrium and a relative humidity <15%. The stepper motor was then used to move the substrate into contact with the end of the nanotube. Finally, force curves were acquired at a fixed scanner velocity of 100 nm sec^{-1}. For all experiments presented herein, the scanner moved 2 μm in each direction (approach and retraction); the initial scanner position was modified to achieve the desired compression of the SWNT. The natural resonance frequency was determined from the thermal spectrum and the spring constant of the SWNT tipped cantilever was calculated using the equipartition theorem [38].

The AFM software was set to record both deflection and oscillation amplitude as a function of scanner displacement in the z dimension. Raw signals (prior to analog filtering) for the vertical deflection, horizontal deflection, and the sum signals were taken from the microscope base into a PCI-6120 data acquisition card through a BNC-2110 interface (National Instruments, Austin, TX, USA) with a data acquisition rate of 800 kHz. To correlate these signals with scanner movement in the z dimension, the z scanner voltage was taken from the signal access module and sent to the data acquisition card. The thermal resonance of the cantilever was measured using a Dynamic Signal Analyzer program written in LabVIEW while simultaneously acquiring the force curve. Briefly, the time dependent vertical deflection signal was converted into the frequency domain using the discrete Fourier transform. The resultant power spectral density (PSD) data was ensemble averaged and displayed in waterfall format. The acquisition time per FFT was 10 ms, the number of averages in each PSD was 16, and the number of PSDs per waterfall plot was 500. With respect to the scanner velocity, each averaged power spectral density plot represents 16 nm of scanner movement. Horizontal deflection and scanner movement were also recorded with respect to time. The reader is referred to the dissertation of Barker for complete details of the experimental system and measurement apparatus [39].

3. Results and Discussion

The adhesive and mechanical response of SWNTs greater than 2 μm in length during both compression and tension were examined. Each SWNT was repeatedly brought into and out of contact with the substrate by extending and retracting the scanner in the z-direction while monitoring cantilever deflection and thermally driven resonance. An example of the SWNTs included in this investigation is provided in Figure 1. The images displayed in this figure depict the same SWNT from two different angles. The results from compression and tension data can be examined in three different ways. For clarity, each of these results is discussed individually.

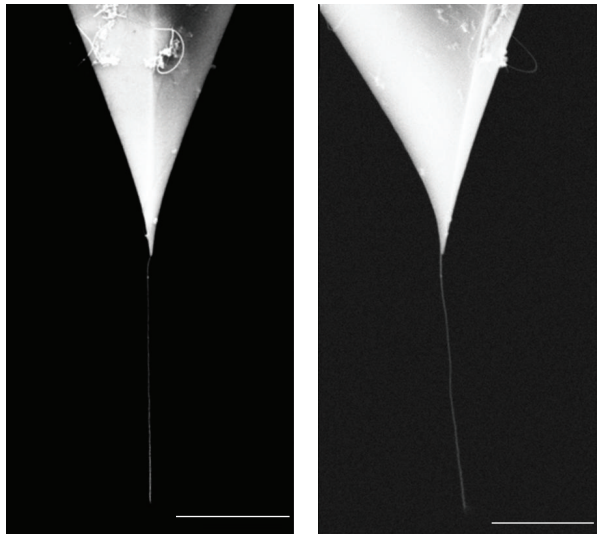

(a) (b)

Figure 1: SEM images looking at the front (a) and the side (b) of one of the carbon nanotube-modified AFM tips used in this study. The scale bar in each image represents 1 μm.

3.1. Nanotube Buckling. Approach of the substrate to the probe was performed in intermittent contact mode. The point of contact is established with a momentary decrease in oscillation amplitude as illustrated in Figure 2(a). Upon retraction the amplitude is even further reduced but only for a brief period and then it quickly returns to the preset drive amplitude. This would suggest that the restorative forces at contact are quickly removed. Figure 2(b) shows a typical force curve acquired with a SWNT tip with reversal of the direction of the scanner movement 60 nm after contact of the probe with the surface and with the drive amplitude of the oscillation set to zero. Note that the sinusoidal pattern in the curve is a resultant of the optical interference from the laser reflecting off both the cantilever and the substrate surface. Also note that there is no measurable deflection of the cantilever during approach and a small but notable downward deflection occurs on scanner retraction. We attribute the zero or little deflection to the high spring constant of the cantilevers (2-3 N/m) relative to the spring constant of the SWNT.

Without changing or stopping scanner movement, the drive voltage for the oscillation amplitude was turned off. Thermal resonance data was then acquired by converting the time dependent vertical deflection signal acquired during the force curve into the frequency domain using the discrete Fourier transform. The resultant PSD data was collected, ensemble averaged, and displayed in waterfall format. Figure 2(c) is waterfall plot for the cantilever resonance associated with the force curve data presented in Figure 2(b). Time and frequency are the in-plane axes, with the amplitude of thermal resonance on the z-axis. In this figure, the scanner approaches the SWNT from 0 to 20 s and retracts from 20 to 40 s. The amplitude is color encoded to help visualize changes. To reduce complexity, the data is presented in an alternative format. The plot presented in Figure 2(d) depicts the frequency of maximum amplitude corresponding to the primary mode of cantilever thermal resonance as a function of time. Superimposed onto this data is the movement of the scanner over the identical time period to enable correlation of changes in frequency with scanner extension. For the experiment shown in Figure 2, the apex of the curve of scanner movement (20 sec) was the moment when the direction of the scanner was reversed and the smallest gap existed between the cantilever tip and substrate. Note that there is no shift in the thermal resonance frequency during approach. A shift of 4 kHz is measured upon retraction indicating that during retraction the nanotube is put into tension.

Contact of the nanotube with the substrate was monitored both by tracking the amplitude of the oscillation when the cantilever is externally driven (Figure 2(a)) or the primary mode resonance frequency when the cantilever was driven only by thermal motion (Figure 2(d)). In both cases, the sudden return to baseline following contact suggests that the nanotube mechanically failed; that is, it buckled. Our interpretation that the nanotube undergoes buckling is in agreement with the similar observations made by Jiang et al. [26]. Using a scanning electron microscope, they clearly saw that compression of multiwalled carbon nanotubes resulted in buckling at short compression distances.

The critical buckling load for our nanotubes was calculated. Applying a clamped-pinned model from the Euler equation to our system, such that the nanotube is clamped at the AFM tip and pinned by adhesive interactions at the surface, yields the critical buckling load, F_{crit}, defined by

$$F_{\text{crit}} = \frac{EI\beta^2}{\left(L_{\text{SWNT}}\right)^2}, \tag{1}$$

where E is the elastic modulus of the SWNT, I is the area moment of inertia, β is a constant determined by the boundary conditions, and L_{SWNT} is the length of the SWNT. For a clamped-pinned column, β is the first nonzero root of the equation $\tan(\beta) = \beta$, or approximately 4.4934 [40]. Using the median values for a SWNT [41, 42], where the outer diameter of the tube is 1.3 nm, an elastic modulus of 1.0 TPa, and a representative length from our samples of 3.0 μm, the critical buckling load is calculated to be 0.6 pN. Using the spring constants of our cantilevers, the critical buckling load is reached in the first nanometer of compression [2, 18, 43]. This strongly suggests that our nanotubes buckle immediately after contact with the surface.

3.2. Tensile Loading. The shift in frequency when the nanotube is put into tension (as shown in Figure 2(d)) can be modeled as two springs in parallel. The nanotube along its long axis is one spring; the AFM cantilever is the other spring, with the effective mass of the cantilever and AFM tip separating the two. The change in resonance frequency, Δf, for such a system is directly related to the ratio of the two

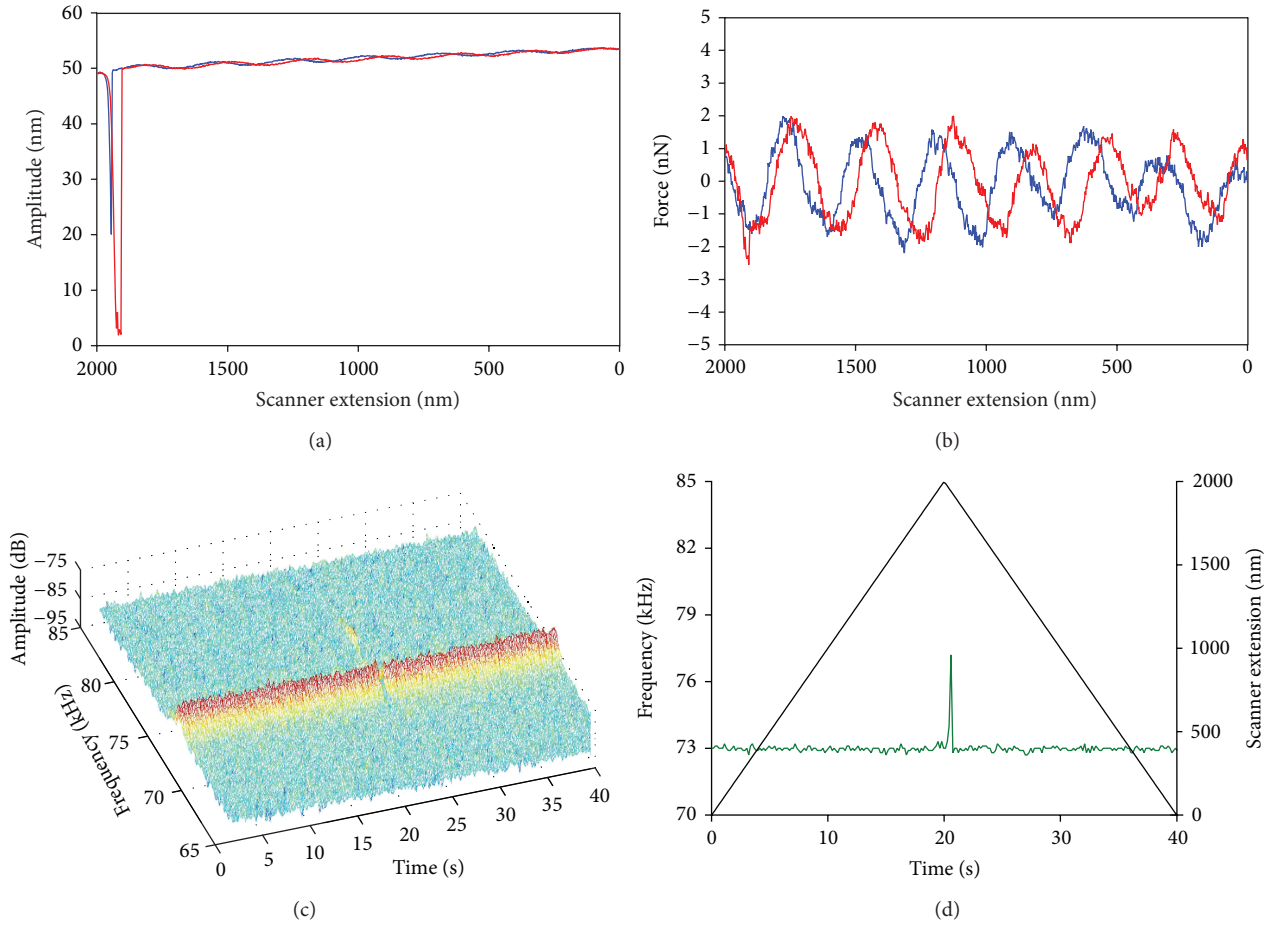

Figure 2: MDFS data: (a) oscillation amplitude of the externally driven cantilever showing approach (blue) and retraction (red); (b) the force-distance curve for the undriven cantilever at the same scan setting in (a); (c) waterfall plot acquired simultaneously with the force curve presented in (b); (d) plot of frequency of maximum amplitude (green) and scanner displacement (black) versus time.

spring constants [17, 18, 44]. For springs in parallel, the change in resonance frequency is given by

$$\frac{\Delta f}{f_0} = \sqrt{1 + \frac{k_{\mathrm{SWNT}}}{k_{\mathrm{CANT}}}} - 1, \tag{2}$$

where f_0 is the thermal resonance frequency of the system in free space and k_{SWNT} and k_{CANT} are the spring constants of the SWNT and cantilever, respectively. In free space, f_0 is dominated by the AFM cantilever spring constant and cantilever's effective mass. The spring constant of the SWNT can be used to determine its elastic modulus, E, such that

$$k_{\mathrm{SWNT}} = \frac{EA}{L_{\mathrm{SWNT}}}, \tag{3}$$

where A is the cross-sectional area and L_{SWNT} is the length of the nanotube.

Figure 3 shows the frequency response of the system as the SWNT probe is slightly compressed (only 50 nm) onto three different surfaces over chemically modified template-stripped gold: methyl-terminated alkanethiol (Figure 3(a)), hydroxy-terminated alkanethiol (Figure 3(b)), and amino-terminated alkanethiol (Figure 3(c)). Under the low compression regime displayed in this figure, no frequency shift is measured during scanner extension. During scanner retraction, the nanotube-cantilever system is put into tension and shifts to a singular frequency. Note that this frequency shift is essentially the same for all three surfaces even though the strengths of adhesion of the SWNT to these surfaces are known to differ [17–19]. If the strength of adhesion is likened to an "adhesive spring," this spring would be in series with the SWNT probe. Since the spring constant of the nanotube is believed to be much smaller than that of the "adhesive spring," the SWNT dominates the equivalent spring constant of the probe/substrate. Thus, the shifted resonant frequency should be largely independent of the strength of adhesion.

To compute the elastic modulus of the SWNT using (3), an accurate measure of tube dimensions is required. Measurement of the length of these long SWNTs was made with a scanning electron microscope. Measurement of tube diameter is best performed with a transmission electron microscope

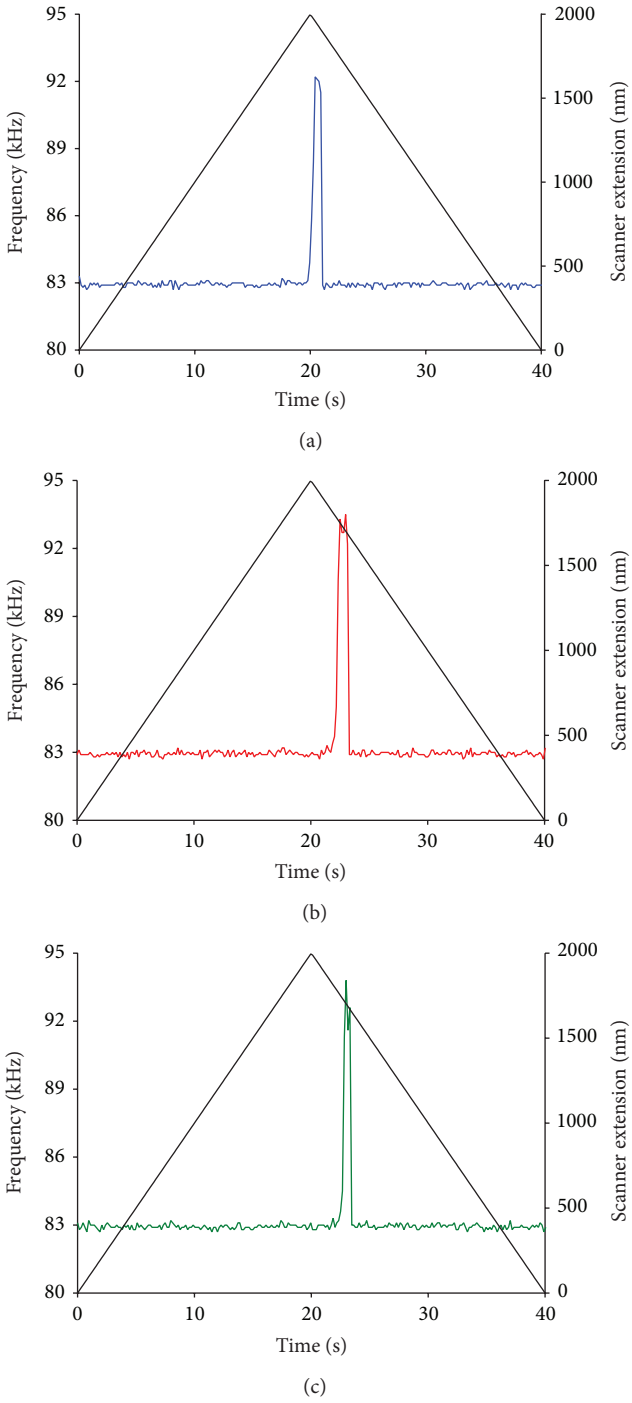

FIGURE 3: Plots of primary resonance mode frequency versus time for three different self-assembled monolayers on template-stripped gold: (a) methyl-terminated alkanethiol, (b) hydroxy-terminated alkanethiol, and (c) amino-terminated alkanethiol. For this dataset, the length of the nanotube was 5.63 μm long. The cantilever resonance frequency was 82.93 kHz and had a spring constant of 1.8 N/m.

(TEM). Our attempts to acquire the latter met with two undesirable outcomes. TEM images prior to mechanical loading experiments resulted in pyrolysis of the tube presumably due to charging effects and poor grounding of the probe while being imaged at high voltages. Pyrolysed nanotubes were no longer suitable for mechanical testing. So we elected to delay TEM imaging until after mechanical loading studies. During this phase of the investigation, the entire inventory of our nanotube-modified AFM tips were separated from the AFM tip. The repeated mechanical stresses incurred during the experiments, including compression to 30% of the length of the nanotube, caused the nanotubes to break at the nanotube/catalyst junction. This fact is illustrated in Figures 4(a) and 4(b). In some instances, detached nanotubes were located on the surface while imaging with the AFM tip to which they were formerly attached, as depicted in Figure 4(c). In this case, tube diameters were determined from heights measured through imaging using the AFM tip to which they were formerly attached.

The cross-sectional area needed in (3) was computed in the following way. An average diameter of 1.4 ± 0.1 nm was found from AFM images of broken nanotube tips. The manufacturer of the SWNT probes claimed that they were single-walled; the measured diameter is consistent with this claim.

Nanotube lengths were determined from SEM images and ranged from 2.0 to 5.7 μm. Using these values and the measured frequency shift, $\Delta f / f_0$, the elastic modulus of the single-walled carbon nanotube is found to be 1.6 ± 1 TPa. This result is in good agreement with previous literature values for the elastic modulus of SWNT [41, 45–47]. The uncertainty in our reported result is due to the precision of frequency measurements and the relative magnitudes of k_{SWNT} and k_{CANT}. In our system, and k_{CANT} is an order of magnitude greater than k_{SWNT}; the uncertainty of the calculated modulus decreases exponentially as the ratio of the spring constants approaches unity [31].

3.3. Friction Analysis. The SWNT tips were also subjected to larger compression displacements. Thermal resonance data for a nanotube brought into and out of contact with amino-terminated alkanethiol-modified gold surface is presented in Figure 5 as the extent of compression is increased. In each graph, the dashed line indicates the point of contact. It is seen that the frequency response changes in magnitude and duration with increasing compression. Figure 5(a) is similar to the previous pattern of contact with immediate buckling during scanner extension, followed by tension during retraction. Figure 5(b) shows the frequency shift as the SWNT was compressed for a distance of 300 nm instead of 50 nm (Figure 5(a)). After initial contact and buckling, the frequency rises and falls with scanner extension. Sudden shifts to higher frequency indicate that the nanotube is pinned on the surface and provides resistance to cantilever oscillation. Sudden shifts to lower frequency indicate that the nanotube buckles and/or slips on the surface, removing this resistance. In Figure 5(b), the nanotube undergoes two distinct slip-stick-buckle events during approach. During retraction, several stick-tension-slip events are observed. The retraction portion of the force curve displays a sawtooth pattern that is indicative of slip-stick motion (data not shown). As the compression on the nanotube is further increased (710 nm),

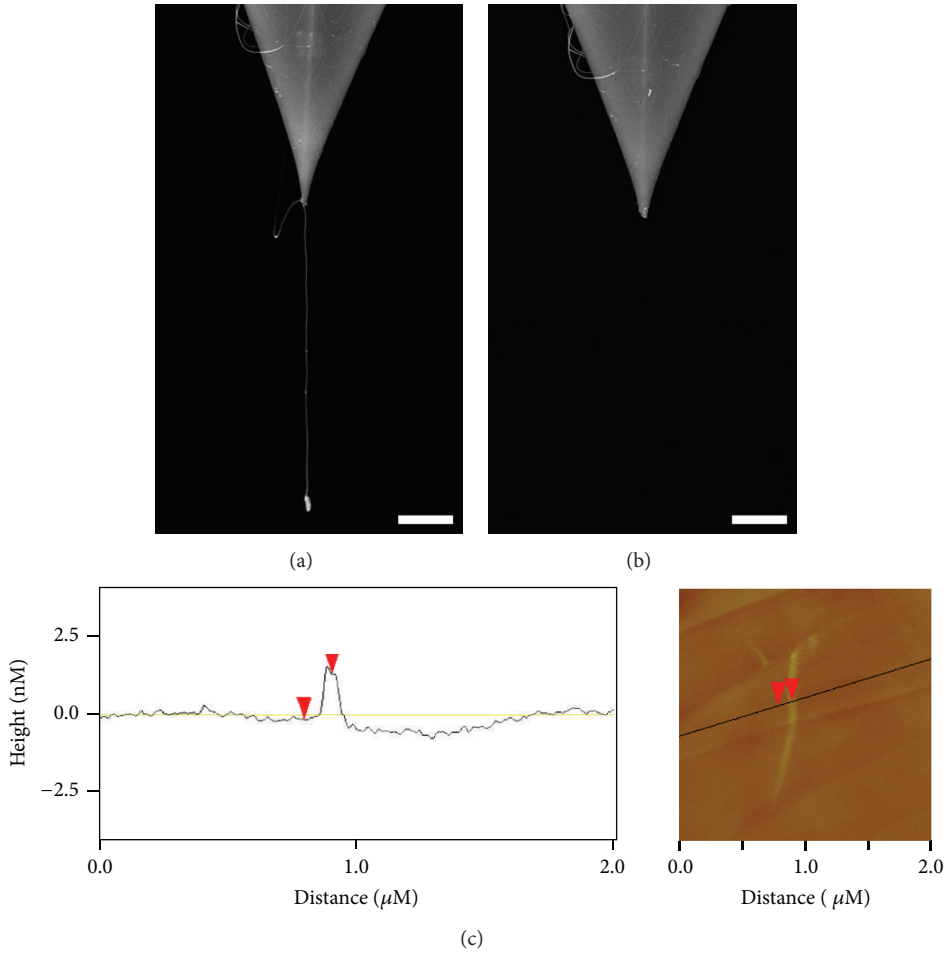

Figure 4: SEM images showing (a) before and (b) after mechanical failure caused by repeated compression. The AFM image (and sectional analysis) of one of the nanotubes that was found after fracture is shown in (c). The image was acquired in intermittent contact mode using the same tip from which it was detached.

additional slip-stick-buckle and stick-tension-slip events are observed (Figure 5(c)). Note that the magnitude of frequency shifts in Figure 5(c) is greater than that found in Figures 5(a) and 5(b).

The slip-stick phenomenon depends upon the chemistry at the SWNT-substrate interface. Figure 6 shows the thermal resonance frequency response for a single SWNT probe brought in and out of contact with three different chemically-modified gold substrates applying approximately the same compression distance. Figure 6(a) depicts the interaction of the SWNT with a methyl-terminated alkanethiol. Minimal shifts in frequency are observed during retraction indicating that the nanotube slides freely on the surface. Figure 6(b) depicts the interaction of the SWNT with a hydroxy-terminated alkanethiol. A measurable frequency shift is observed consistent with an increased affinity of the nanotube for the hydroxy-terminated surface. Figure 6(c) depicts the interaction of the SWNT with an amino-terminated alkanethiol. The frequency response for this surface is larger than for the hydroxyl-terminated surface. Taken collectively, the data presented in Figures 5 and 6 suggests that the number and extent of slip events is indicative of the strength of adhesion between the nanotube and the surface; that is, –CH3 < –OH < –NH2. This trend is consistent with previously published adhesion measurements [20, 30, 32–34, 40]. The results in Figures 3 and 6 may, at first glance, appear to be in conflict. At minimal compression, the SWNT buckles but does not slip. In the absence of slip, the surface chemistry has no effect on the frequency response of the system. In the presence of slip, nanotube-substrate chemistry mediates the extent and duration of the observed frequency shifts. Differences in the chemistry of the interface can be distinguished after compression-induced buckling and slip. Thus, there is no conflict between the data presented in the two figures.

Interestingly, after the buckling event (the system is now described as postbuckled), the force required to overcome the adhesion at the pinned end of the nanotube and enter the slip-stick domain is, by definition, the frictional force. A prediction can be made about the shape of the buckled nanotube as it undergoes further compression by applying an elastica model of a postbuckled column [36, 39].

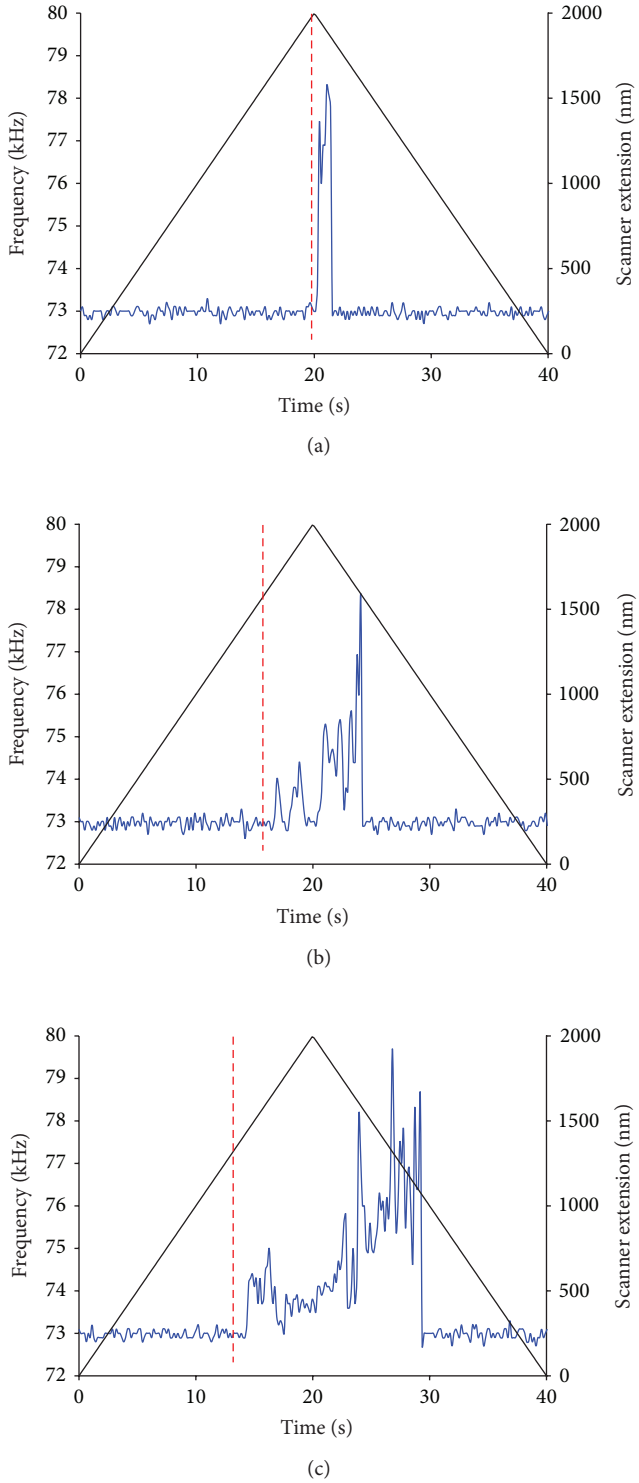

Figure 5: Plots of primary resonance mode frequency versus time for a SWNT compressed for three different distances on an amino-terminated alkanethiol monolayer: (a) 50 nm, (b) 300 nm, and (c) 710 nm. The dashed line indicates the contact point of the nanotube with the substrate. For this dataset, the length of the nanotube was 2.96 μm long. The cantilever resonance frequency was 72.99 kHz and had a spring constant of 2.5 N/m.

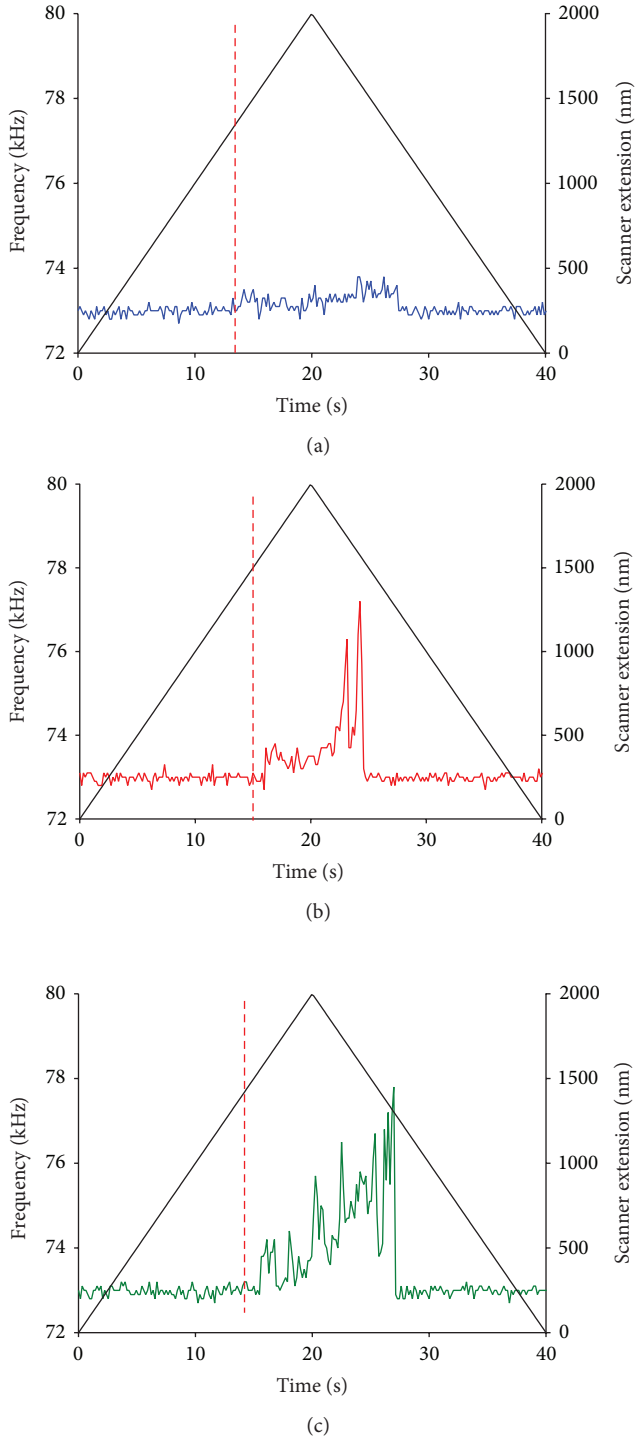

Figure 6: Plots of primary resonance mode frequency versus time at large compression for (a) methyl-terminated alkanethiol, (b) hydroxyl- terminated alkanethiol, and (c) amino-terminated alkanethiol, on template-stripped gold. The dashed line indicates the contact point estimated from the oscillation amplitude when the system was externally driven. For this dataset, the length of the nanotube was 2.96 μm long. The cantilever resonance frequency was 72.99 kHz and had a spring constant of 2.5 N/m.

The boundary conditions for this problem correspond to a clamped-pinned configuration: zero displacement and rotation at the clamped end and zero moment at the substrate. It is assumed that the contact point is directly beneath the AFM tip; however, the probe tip can be moved to the left or right by varying x. The differential equations and associated boundary conditions were solved using the Matlab solver for boundary-value problems, bvp4c, as previously described [36, 39]. Through the solution of the boundary-value problem, the horizontal and vertical forces at the pinned endpoint can be calculated at different compression steps. The distance from the AFM tip to the substrate surface is varied through choice of the boundary condition.

Figure 7 shows the evolution of the nanotube shape as the scanner height is raised; that is, the tip to substrate distance is decreased. Note in particular how the angle θ that the nanotube makes with the normal to the substrate is predicted to increase as the nanotube becomes more and more buckled. This trend is further revealed in Figure 8, which shows the angle θ as a function of the normalized scanner height. Note that when the scanner displacement is near 30% of the nanotube length, it is predicted that the postbuckled shape will meet the substrate at near 90° angle. The variation in the angle predicted by this model can be used to determine the friction coefficient as described below.

At the substrate surface, the horizontal force, P_H, is equivalent in magnitude to the force of static friction, F_f, and the vertical load, P_V, is equivalent to the magnitude of the normal force, F_N. Since the moment at the substrate-end of the elastica is zero, it can be shown that

$$\frac{F_f}{F_N} = \tan\theta. \tag{4}$$

It is important to note that (4) holds regardless of whether the normal load is due to elastic deformation of the SWNT or due to adhesion, or both. A corollary to (4) is that the coefficient of friction, μ, necessary to prevent slip can be found using the relation

$$F_f \leq \mu F_N. \tag{5}$$

In other words, $\mu \geq \tan\theta$.

For each compression step, the minimum coefficient of friction required to keep the tube pinned can be calculated using (5). As compression increases, the angle θ increases and, consequently, the minimum coefficient of static friction must increase if the nanotube is to remain pinned to the surface.

Figure 9 shows the minimum coefficient of friction as a function of the normalized scanner height. The middle (blue) curve corresponds to the nominal case where the substrate is perpendicular to the z-axis. Inclining the substrate will either inhibit or favor slip; the neighboring lines in Figure 9 correspond to ±1 degree rotation of the substrate. Figure 9 can be used to estimate the friction coefficient between the nanotube and substrates having various chemical coatings.

Specifically, the scanner extension and cantilever displacement can be monitored in an experiment until the first slip event is detected. The relative change in the distance between the AFM tip and the surface (normalized by the undeformed probe length) at the first slip event is used as the abscissa value in Figure 9 to yield the coefficient of friction.

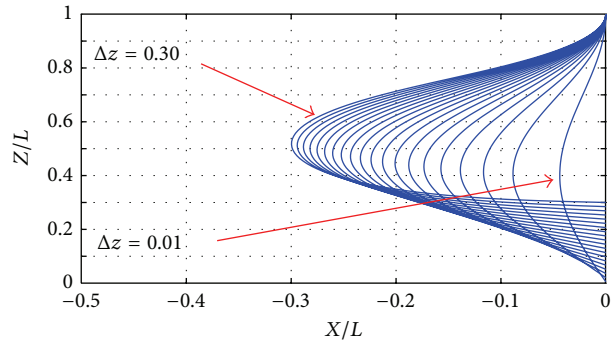

Figure 7: Postbuckled elastica shape as the AFM tip to substrate distance is changed. Δz is the change in the AFM tip to substrate distance normalized by the original, undeformed length of the nanotube.

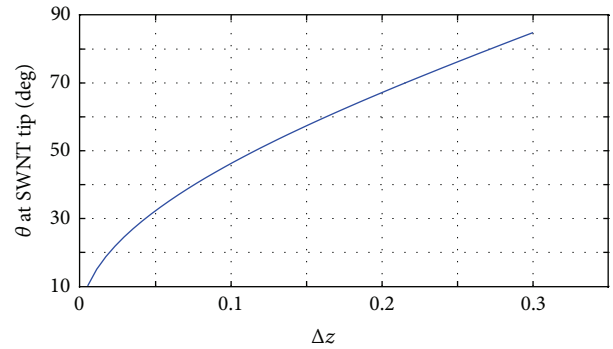

Figure 8: Predicted angle between the elastica and the normal to the vertical at the point of contact between the nanotube and the substrate.

The procedure described above was used to estimate the coefficient of friction for three surfaces of self-assembled monolayers on template-stripped gold. For the methyl-terminated monolayer (11-undecanethiol), the coefficient of friction was found to be 0.11; an uncertainty of 1 degree in the nominal surface angle yields an uncertainty of ±0.02. Similarly, the friction coefficients were estimated to be 0.34 ± 0.02, and 0.47 ± 0.02 for 11-hydroxyl-, and 11-amino- undecanethiol, respectively. These results are in the ranges seen by others who worked on friction of Si_xN_y AFM tips and self-assembled monolayers and different carbon materials [20, 27, 28, 35, 48].

4. Conclusions

In this report, we demonstrate the advantages MDFS offers to studying mechanical responses and adhesive interactions at the nanoscale. By monitoring the shift in the thermal resonance frequency, MDFS enables the calculation of the spring constant and elastic modulus of carbon nanotubes under ambient conditions. This approach delineated herein

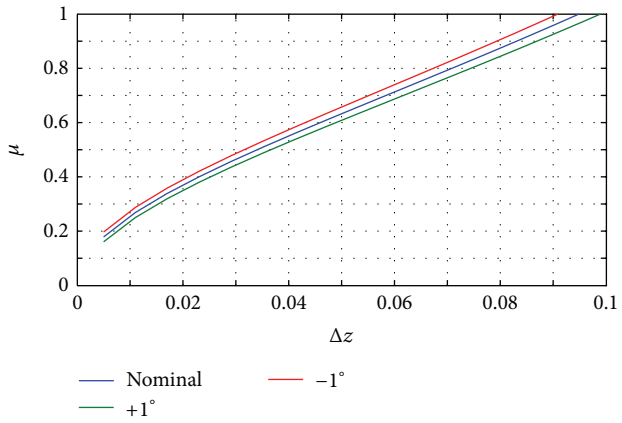

FIGURE 9: Minimum coefficient of friction versus normalized probe end position. Blue line is for a nominally flat substrate; green and red lines correspond to substrates inclined +1 and −1 degrees, respectively.

is not limited to SWNTs; it is directly applicable to a wide variety of nanoobjects including nanorods, nanofibers, and biomolecules under tension. Additionally, an elastica model of the postbuckled state of the nanotube has been developed. By monitoring the location of the frequency shift in thermal resonance, the static coefficient of friction has been calculated from experiments performed on three different chemically-modified surfaces. The results presented herein are, to our knowledge, the first static friction results for carbon nanotubes on self-assembled monolayers. The observed trend in the dependence of the coefficient of friction with the identity of the terminal group on the monolayer follows the same trend previously observed for the strength of adhesion between a SWNT and an alkanethiol-modified surface [40, 49].

In a broader context, this work cautions that high aspect ratio nanotube probes buckle under minimal compressive loads. Nanotube buckling leads to imaging artifacts [5, 25, 30, 50, 51]. Imaging in intermittent contact mode does not, necessarily, prevent this artifact. As demonstrated in Figure 2(a), a buckled nanotube does not necessarily dampen cantilever oscillation. Proper imaging protocol requires acquisition of an oscillation amplitude plot and setting the set point value to the first point of cantilever damping. The spring constant of the cantilever must also be carefully chosen. Equation (1) predicts the force at which a SWNT buckles. We suggest the following equation for choosing a cantilever with spring constant k_{CANT} so that it will not cause a nanotube with an aspect ratio, A_R, and outer diameter, d, to buckle after contact and 10 nm of axial compression:

$$k_{\mathrm{CANT}} < \frac{Ed^2}{A_R^2}\left(9.3 \times 10^7\ \mathrm{m}^{-1}\right). \tag{6}$$

This equation treats the SWNT as a column whose inner diameter is half of its outer diameter because that approximates the relationship for SWNTs. During intermittent contact mode imaging, it is possible that the nanotube can experience compressive loads up to 10 nN. The constant at the end of the equation is the product of all other constants and allows the remaining variables to be calculated using SI units. Without careful consideration of the spring constant of the AFM cantilever relative to the critical buckling load, high aspect ratio carbon nanotube AFM probes will buckle during imaging, even in intermittent contact mode.

Conflict of Interests

The authors declare that there is no conflict of interests regarding the publication of this paper.

Acknowledgments

The authors acknowledge fruitful discussions with Professor Jonathan Colton and Dr. Andrew MacFarland concerning the mechanical models for their system. They thank Nick Schacher from NanoDevices for providing them with the nanotube-tipped cantilevers and Jean Jarvaise formerly from Veeco Instruments Metrology Division for guidance in modifying the electronics of the NanoScope IIIA. M. A. Poggi gratefully acknowledges a fellowship from the NASA Graduate Student Researchers Program (NGT-1-02002). This research was made possible by Grants from the National Institutes of Health (EB000767) and the National Science Foundation (CMMI1130739).

References

[1] T. DeBorde, J. C. Joiner, M. R. Leyden, and E. D. Minot, "Identifying individual single-walled and double-walled carbon nanotubes by atomic force microscopy," *Nano Letters*, vol. 8, no. 11, pp. 3568–3571, 2008.

[2] M. R. Falvo, G. J. Clary, R. M. Taylor II et al., "Bending and buckling of carbon nanotubes under large strain," *Nature*, vol. 389, no. 6651, pp. 582–584, 1997.

[3] M.-F. Yu, O. Lourie, M. J. Dyer, K. Moloni, T. F. Kelly, and R. S. Ruoff, "Strength and breaking mechanism of multiwalled carbon nanotubes under tensile load," *Science*, vol. 287, no. 5453, pp. 637–640, 2000.

[4] R. M. Stevens, "New carbon nanotube AFM probe technology," *Materials Today*, vol. 12, no. 10, pp. 42–45, 2009.

[5] N. R. Wilson and J. V. MacPherson, "Carbon nanotube tips for atomic force microscopy," *Nature Nanotechnology*, vol. 4, no. 8, pp. 483–491, 2009.

[6] C. P. Collier, "Carbon nanotube tips for scanning probe microscopy," in *Carbon Nanotubes: Properties and Applications*, M. J. O'Connell, Ed., pp. 295–314, CRC Press, Boca Raton, Fla, USA, 2006.

[7] S. S. Wong, J. D. Harper, P. T. Lansbury Jr., and C. M. Lieber, "Carbon nanotube tips: high-resolution probes for imaging biological systems," *Journal of the American Chemical Society*, vol. 120, no. 3, pp. 603–604, 1998.

[8] C. V. Nguyen, Q. Ye, and M. Meyyappan, "Carbon nanotube tips for scanning probe microscopy: fabrication and high aspect ratio nanometrology," *Measurement Science & Technology*, vol. 16, no. 11, pp. 2138–2146, 2005.

[9] E. D. de Asis Jr., J. Leung, and C. V. Nguyen, "Carbon nanotube tips in atomic force microscopy with applications to imaging

in liquid," in *Atomic Force Microscopy in Liquid: Biological Applications*, pp. 35–64, Wiley-VCH, Weinheim, Germany, 2012.

[10] I. R. Shapiro, S. D. Solares, M. J. Esplandiu, L. A. Wade, W. A. Goddard, and C. P. Collier, "Influence of elastic deformation on single-wall carbon nanotube atomic force microscopy probe resolution," *The Journal of Physical Chemistry B*, vol. 108, no. 36, pp. 13613–13618, 2004.

[11] Q. M. Hudspeth, K. P. Nagle, Y.-P. Zhao et al., "How does a multiwalled carbon nanotube atomic force microscopy probe affect the determination of surface roughness statistics?" *Surface Science*, vol. 515, no. 2-3, pp. 453–461, 2002.

[12] S. I. Lee, S. W. Howell, A. Raman, R. Reifenberger, C. V. Nguyen, and M. Meyyappan, "Complex dynamics of carbon nanotube probe tips," *Ultramicroscopy*, vol. 103, no. 2, pp. 95–102, 2005.

[13] M. C. Strus, A. Raman, C.-S. Han, and C. V. Nguyen, "Imaging artefacts in atomic force microscopy with carbon nanotube tips," *Nanotechnology*, vol. 16, no. 11, pp. 2482–2492, 2005.

[14] L. A. Wade, I. R. Shapiro, Z. Ma, S. R. Quake, and C. P. Collier, "Correlating AFM probe morphology to image resolution for single-wall carbon nanotube tips," *Nano Letters*, vol. 4, no. 4, pp. 725–731, 2004.

[15] S.-I. Yang, "Structural study using ultrahigh resolution carbon nanotube AFM probe tips," *Journal of the Korean Chemical Society*, vol. 49, no. 6, pp. 517–520, 2005.

[16] L. Zhang, E. Ata, S. C. Minne, and P. Hough, "Single-walled carbon nanotube probes for AFM imaging," in *Proceedings of the 17th IEEE International Conference on Micro Electro Mechanical Systems (MEMS '04)*, pp. 438–441, Maastricht, The Netherlands, January 2004.

[17] J. Buchoux, J.-P. Aimé, R. Boisgard, C. V. Nguyen, L. Buchaillot, and S. Marsaudon, "Investigation of the carbon nanotube AFM tip contacts: free sliding versus pinned contact," *Nanotechnology*, vol. 20, no. 47, Article ID 475701, 2009.

[18] J. Buchoux, L. Bellon, S. Marsaudon, and J.-P. Aimé, "Carbon nanotubes adhesion and nanomechanical behavior from peeling force spectroscopy," *European Physical Journal B*, vol. 84, no. 1, pp. 69–77, 2011.

[19] D. Jarzabek, Z. Rymuza, and N. Ohmae, "Friction and adhesion of carbon nanotube brushes," *International Journal of Materials Research*, vol. 100, no. 7, pp. 973–977, 2009.

[20] J. Lievonen and M. Ahlskog, "Lateral force microscopy of multiwalled carbon nanotubes," *Ultramicroscopy*, vol. 109, no. 7, pp. 825–829, 2009.

[21] C. L. Cheung, J. H. Hafner, T. W. Odom, K. Kim, and C. M. Lieber, "Growth and fabrication with single-walled carbon nanotube probe microscopy tips," *Applied Physics Letters*, vol. 76, no. 21, pp. 3136–3138, 2000.

[22] A. Kutana, K. P. Giapis, J. Y. Chen, and C. P. Collier, "Amplitude response of single-wall carbon nanotube probes during tapping mode atomic force microscopy: modeling and experiment," *Nano Letters*, vol. 6, no. 8, pp. 1669–1673, 2006.

[23] S. I. Lee, S. W. Howell, A. Raman, and R. Reifenberger, "Nonlinear dynamics of microcantilevers in tapping mode atomic force microscopy: a comparison between theory and experiment," *Physical Review B*, vol. 66, no. 11, Article ID 115409, 10 pages, 2002.

[24] S. I. Lee, S. W. Howell, A. Raman, and R. Reifenberger, "Nonlinear dynamic perspectives on dynamic force microscopy," *Ultramicroscopy*, vol. 97, no. 1–4, pp. 185–198, 2003.

[25] S. I. Lee, S. W. Howell, A. Raman, R. Reifenberger, C. V. Nguyen, and M. Meyyappan, "Nonlinear tapping dynamics of multiwalled carbon nanotube tipped atomic force microcantilevers," *Nanotechnology*, vol. 15, no. 5, pp. 416–421, 2004.

[26] A. N. Jiang, S. Gao, X. L. Wei, X. L. Liang, and Q. Chen, "Amplitude response of multiwalled carbon nanotube probe with controlled length during tapping mode atomic force microscopy," *The Journal of Physical Chemistry C*, vol. 112, no. 40, pp. 15631–15636, 2008.

[27] B. Bhushan and X. Ling, "Adhesion and friction between individual carbon nanotubes measured using force-versus-distance curves in atomic force microscopy," *Physical Review B*, vol. 78, no. 4, Article ID 045429, 9 pages, 2008.

[28] B. Bhushan, X. Ling, A. Jungen, and C. Hierold, "Adhesion and friction of a multiwalled carbon nanotube sliding against single-walled carbon nanotube," *Physical Review B*, vol. 77, no. 16, Article ID 165428, 12 pages, 2008.

[29] S. D. Solares, M. J. Esplandiu, W. A. Goddard III, and C. P. Collier, "Mechanisms of single-walled carbon nanotube probe-sample multistability in tapping mode AFM imaging," *The Journal of Physical Chemistry B*, vol. 109, no. 23, pp. 11493–11500, 2005.

[30] M. A. Poggi, J. S. Boyles, L. A. Bottomley et al., "Measuring the compression of a carbon nanospring," *Nano Letters*, vol. 4, no. 6, pp. 1009–1016, 2004.

[31] B. Bhushan and H. Liu, "Nanotribological properties and mechanisms of alkylthiol and biphenyl thiol self-assembled monolayers studied by AFM," *Physical Review B*, vol. 63, no. 24, Article ID 245412, 11 pages, 2001.

[32] D. Chabrier, B. Bhushan, and S. Marsaudon, "Humidity effect on the interaction between carbon nanotubes and graphite," *Applied Surface Science*, vol. 256, no. 14, pp. 4672–4676, 2010.

[33] M. A. Poggi, P. T. Lillehei, and L. A. Bottomley, "Chemical force microscopy on single-walled carbon nanotube paper," *Chemistry of Materials*, vol. 17, no. 17, pp. 4289–4295, 2005.

[34] G. Rius and M. Yoshimura, "Cooperative multiwalled carbon nanotubes for enhanced force spectroscopy," *e-Journal of Surface Science and Nanotechnology*, vol. 10, pp. 341–345, 2012.

[35] M. Ishikawa, M. Yoshimura, and K. Ueda, "A study of friction by carbon nanotube tip," *Applied Surface Science*, vol. 188, no. 3-4, pp. 456–459, 2002.

[36] K. M. Barker, A. Ferri, and L. A. Bottomley, "Adhesive and mechanical properties of carbon nanotube probes contacting chemically-treated turfaces," in *Proceedings of the ASME International Mechanical Engineering Congress and Exposition (IMECE '11)*, vol. 11 of *ASME Conference Proceedings*, pp. 739–746, Denver, Colorado, USA, November 2011.

[37] E. Yenilmez, Q. Wang, R. J. Chen, D. Wang, and H. Dai, "Wafer scale production of carbon nanotube scanning probe tips for atomic force microscopy," *Applied Physics Letters*, vol. 80, no. 12, pp. 2225–2227, 2002.

[38] H.-J. Butt and M. Jaschke, "Calculation of thermal noise in atomic force microscopy," *Nanotechnology*, vol. 6, no. 1, pp. 1–7, 1995.

[39] K. M. Barker, *Adhesion of nano-objects to chemically modified surfaces [Ph.D. dissertation]*, Georgia Institute of Technology, Atlanta, Ga, USA, 2009.

[40] R. W. Friddle, M. C. Lemieux, G. Cicero et al., "Single functional group interactions with individual carbon nanotubes," *Nature Nanotechnology*, vol. 2, no. 11, pp. 692–697, 2007.

[41] R. S. Ruoff, D. Qian, and W. K. Liu, "Mechanical properties of carbon nanotubes: theoretical predictions and experimental measurements," *Comptes Rendus Physique*, vol. 4, no. 9, pp. 993–1008, 2003.

[42] A. Sears and R. C. Batra, "Macroscopic properties of carbon nanotubes from molecular-mechanics simulations," *Physical Review B*, vol. 69, no. 23, Article ID 235406, 10 pages, 2004.

[43] C. Q. Ru, "Effective bending stiffness of carbon nanotubes," *Physical Review B*, vol. 62, no. 15, pp. 9973–9976, 2000.

[44] M. Ishikawa, R. Harada, N. Sasaki, and K. Miura, "Adhesion and peeling forces of carbon nanotubes on a substrate," *Physical Review B*, vol. 80, no. 19, Article ID 193406, 4 pages, 2009.

[45] A. P. M. Barboza, H. Chacham, and B. R. A. Neves, "Universal response of single-wall carbon nanotubes to radial compression," *Physical Review Letters*, vol. 102, no. 2, Article ID 025501, 4 pages, 2009.

[46] X. Chen, S. Zhang, D. A. Dikin et al., "Mechanics of a carbon nanocoil," *Nano Letters*, vol. 3, no. 9, pp. 1299–1304, 2003.

[47] R. S. Ruoff and D. C. Lorents, "Mechanical and thermal properties of carbon nanotubes," *Carbon*, vol. 33, no. 7, pp. 925–930, 1995.

[48] C. M. Mate, "Nanotribology studies of carbon surfaces by force microscopy," *Wear*, vol. 168, no. 1-2, pp. 17–20, 1993.

[49] M. A. Poggi, L. A. Bottomley, and P. T. Lillehei, "Measuring the adhesion forces between alkanethiol-modified AFM cantilevers and single walled carbon nanotubes," *Nano Letters*, vol. 4, no. 1, pp. 61–64, 2004.

[50] J. E. Koehne, R. M. Stevens, T. Zink et al., "Using carbon nanotube probes for high-resolution three-dimensional imaging of cells," *Ultramicroscopy*, vol. 111, no. 8, pp. 1155–1162, 2011.

[51] M. Munz, J.-H. Kim, O. Krause, and D. Roy, "Imaging surfaces of nano-scale roughness by atomic force microscopy with carbon nanotubes as tips: a comparative study," *Surface and Interface Analysis*, vol. 43, no. 11, pp. 1382–1391, 2011.

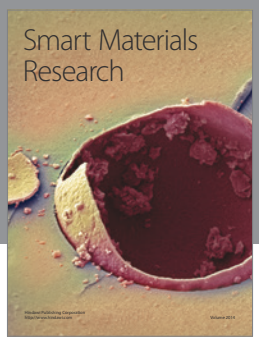

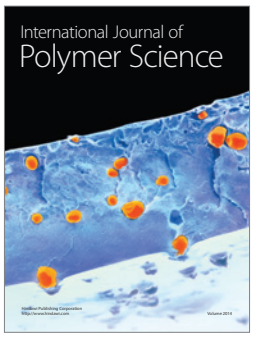

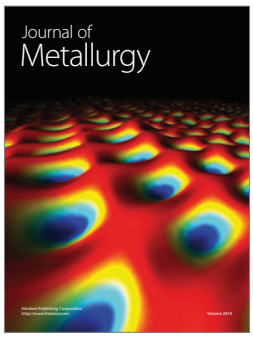

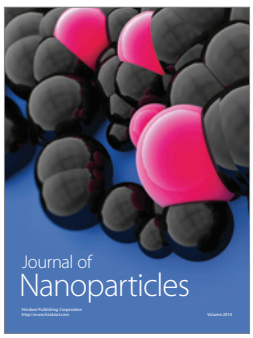

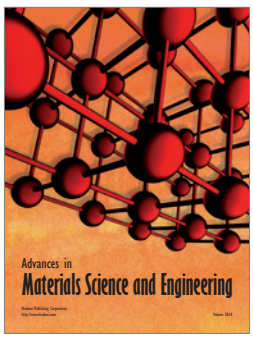

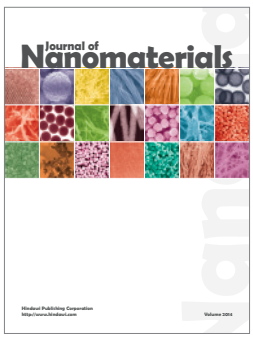

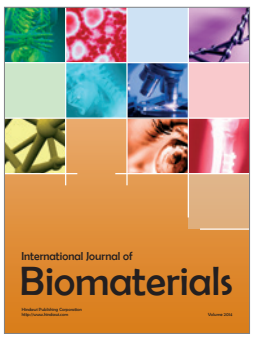

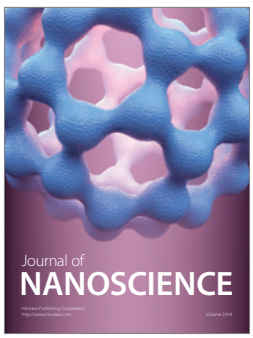

Hindawi

Submit your manuscripts at
http://www.hindawi.com